EVALUATION OF THE NEARSHORE IMPACT OF A HYBRID WAVE-WIND ENERGY FARM

DIACONU Sorin*, ONEA Florin, RUSU Eugen
Department of Applied Mechanics, Dunarea de Jos University of Galati, Romania
*Corresponding author: S. Diaconu, Department of Applied Mechanics, Dunarea de Jos University of Galati, 800201 Galati, Romania.
E-mail address: sorin.diaconu@ugal.ro

ABSTRACT
The main objective of the present work is to evaluate the coastal impact of a hybrid wave-wind farm that would operate in the Romanian nearshore. The target area was chosen in the proximity of the Danube Delta. The simulations performed with the SWAN spectral model were focused on three main objectives: a) analysis in the geographical space of the influence induced by the hybrid farm; b) variations of the incident wave field on the contact with the wave-wind configuration line; and c) influence of the hybrid farm on the shoreline dynamics.

Finally, it was observed that in the presence of the hybrid wave-wind farm for the average wave conditions the impact in the geographical space is rather insignificant with more significant variations for the nearshore currents, while for the second and more energetic case study the wave fields between the hybrid farm and the shoreline are significantly reduced.

Key Words: Black Sea, SWAN, hybrid energy farm, nearshore currents, coastal impact.

1. INTRODUCTION

The erosion processes reported for the Romanian coast have been monitored for decades, and currently they are considered a major issue for this area not only because of the severity of this phenomenon, but more important because of the lack of efficient actions to reduce it. From previous studies it was highlighted the fact that in this area almost 80ha/year of beaches disappear, being caused by a constant retreat of the shoreline to inland (with almost 240m) during the last 40 years (Marchand, 2010; PRC, 2009). During the winter season the erosion process tends to become even more severe, because of the frequent and intense storms which are representative events for this area (Gâştescu and Driga, 2012).

A deeper understanding of the physical processes which occur in the marine environment, especially in the coastal area, can be made through numerical models (Li et al., 2011; Liang et al., 2012). For this purpose, SWAN (Simulating Waves Nearshore) model represents a valuable tool since has the capacity to provide reliable results in the field of coastal protection, being already implemented

in various regions of the world (Stockdon et al., 2012; Strauss et al., 2007). For the Black Sea basin, this model has been mainly used to evaluate the spatial distribution of the wave energy, while recently several case studies were focused on the sediment transport from the vicinity of the Romanian shoreline (Dan et al., 2007; Rusu and Măcuță, 2009).

In order to assess the environmental conditions in the absence of in situ measurements, one alternative to calibrate and validate the numerical simulations is to consider remotely sensed data. The accuracy of the satellite measurements was greatly improved during the last years being currently used in various marine activities (Yin et al., 2010; Yang et al., 2010).

On a large scale the most used engineering solutions to protect the coastal environment from erosion is to create artificial reefs or rock walls, which can be quite expensive and also to produce a negative impact on the natural character of the local environment. From this perspective, considering the increasing development of the systems for the wave energy extraction, a viable solution is to develop energy farms in the marine environment to protect the coastline and to obtain in the same time green energy.

Wind farm projects are suitable to be developed in offshore regions, because of the limited land areas available for such projects and also due to the fact that the wind conditions are usually more energetic in the marine areas (EWEA, 2012; Snyder and Kaiser, 2009). Recent analyses of the wind conditions carried out for the entire Black Sea basin (Onea and Rusu, 2012), suggested that the north-western part of the sea is suitable for efficient operations of the offshore wind farm projects, especially during the winter season. In the same time, the western part of the sea is also considered as being more energetic from the point of view of the wave conditions (Rusu, 2009, Rusu, 2010b, Rusu and Ivan, 2010), in the context of the development of the wave energy converters (WECs), it can be expected that in the near future wave farms will be also implemented, eventually in hybrid wave-wind projects.

Motivated by the above results, the objective of the present work is to evaluate the influence of a potential hybrid wave-wind farm on the local wave fields and nearshore circulation patterns near the sector St. Gheorghe-Buhta located in the Romanian coastal environment.

2. METHODS AND MATERIALS

2.1 Theoretical background of the numerical models considered

Spectral phase averaged models provide nowadays the most accurate estimation of the wave fields on large geographical areas. SWAN (Simulating Waves Nearshore, Booij et al., 1999), is considered the state of the art tool in the wave simulations.

SWAN solves the spectral energy balance equation which describes the evolution of the wave spectrum in time, geographical and spectral domains. The spectral action balance equation is given by:

$$\frac{\partial N}{\partial t}+\nabla\left[\left(\vec{c}_g+\vec{U}\right)N\right]+\frac{\partial}{\partial\sigma}c_\sigma N+\frac{\partial}{\partial\theta}c_\theta N=\frac{S}{\sigma} \qquad (1)$$

where: N is the density spectrum and $\vec{U}$ is the velocity of the ambient current; C_g, C_σ, and C_θ represents the propagation speeds in the frequency space (σ) and geographical space (θ), respectively; S and σ

represents the source and sink terms which are considered in deep water for various processes, as wave-wave interactions, wave generated by wind and whitecapping dissipation. The model also offers the possibility to include formulations referring to shallow water processes such as triad non-linear interactions, diffraction, reflections, bottom friction, and depth-induced wave breaking.

Since the physical processes can be adjusted for each simulation, this model has the capacity to simulate wave conditions from either shallow or deep water. Better predictions of the wave characteristics are possible by calibrating the model with an appropriate combination of physical processes and parameters, which can be identified for a particular site.

From the processes taking place in the surf zone, the generation and propagation of longshore currents can be considered as the most relevant since this is directly involved in modeling the shoreline configuration. In order to predict such currents, various numerical models were developed based on the radiation stress theory to provide an estimation of the current velocity (Longuet-Higgins, 1970).

The prediction system SHORECIRC (Svendsen et al., 2002) is frequently used for the nearshore currents, while a simpler and considerably faster model is Navy Standard Surf Model (NSSM), which includes a parametric relation for cross-shore growth and dissipation of waves due to breaking (Mettlach et al., 2002).

A comprehensive evaluation of the waves and on the corresponding wave induced currents in the nearshore was performed by Conley and Rusu (2006a and 2006b) by joining the SWAN and NSSM model into a versatile computational tool named as the *Interface for SWAN and Surf Models* (ISSM), which can be used for a large number of coastal applications. The reliability and the efficiency of the ISSM modeling system has been already proven based on the comparisons with in situ measurements and with the SHORECIRC circulation model (Rusu and Guedes Soares, 2010), therefore in the present work this modeling system will be used.

The target area considered in the present work (Figure 1) is located on the Romanian nearshore sector St. Gheorghe-Buhta (south of Sulina channel) and this selection is based on the fact that previous studies (Rusu, 2010a) suggested that this area represents a hot spot from the point of view of the wave energy.

The computational domain used in the present simulations is defined by a rectangle with a length of about 17.5km in *x*-direction (cross shore) and 20km in *y*-direction (long shore), more details regarding the target area and the local bathymetry being provided in Figure 2. In order to simulate the presence of the hybrid wave-wind farm, the devices were geometrically defined in the SWAN model as obstacles (also presented in Figure 2).

2.2 Description of hybrid wind-wave farm configuration

The hybrid wave-wind farm considered in the present study (Figure 3a) is composed of 10 wind turbine towers and 50 NEMOS WEC devices distributed on a single line (denoted as N10), which is oriented parallel with the Romanian coastline at water depths in the range of 15-25m. The spatial configuration of the wind turbine array is similar to the one from the offshore wind farm Horns Rev

(North Sea) where the distance between each Vestas V80 wind turbine is almost 560m, while for the wind tower a diameters of 4m was considered (ELSAM, 2002).

The NEMOS device (Figure 3b, NEMOS, 2012) is designed to use the infrastructure of existing offshore wind park by converting the wave energy from these areas into electricity. Although this WEC system is in the early stage of development, it is expected that for one single wind turbine maximum 5 NEMOS units to be installed, each system being defined by a square length of 20x4m (Figure 3c). The distance between each NEMOS device is set at 25m, while a 30m distance to the wind turbine was considered viable for the current simulations. The above details are based on preliminary tests on a small scale NEMOS device, being expected that on the finalization of the test procedure a final configuration to be defined. More details about the NEMOS system and can be found on the project web page (NEMOS, 2012).

2.3 Wave conditions in the target area

One of the most important instruments of a satellite is the altimeter which measures the distance from the satellite to the sea surface by using high frequency signals. For the wave measurements, the results are provided in terms of significant wave heights (denoted with *Hs*), which represents the average of the 1/3 largest waves in the record

Usually the performance of an altimeter is a compromise between a spatial and a temporal resolution, which depends mostly on the satellite trajectory. To reduce this inconvenient, one solution is to consider data coming from various missions. Such a high quality data source is provided by AVISO (Archiving, Validation and Interpretation of Satellite Oceanographic Data), which from 2011 started to develop a multi-mission project which combine data from multiple satellites interconnected (with the Topex/Poseidon mission as a reference).

This multi-mission system collects data from all the satellites, correcting any errors which occur from the movement on the orbit or from significant differences which may exist between the data sets (Dibarboure et al., 2006). The method used to obtain the *Hs* values is based on a nonparametric fits which provide measurements with an accuracy of about 1-2cm (Gaspar et al., 2002).

In order to provide a general overview of the wave conditions from the target area, a comprehensive analysis of the satellite measurements from the AVISO website (http://las.aviso.oceanobs.com), is carried out by considering data available for the time interval: December 2005-July 2012. Thus, in Figure 4 it is presented the spatial distribution of the *Hs* values (for the entire time period) corresponding to a region located in the proximity of the target area. By considering the evolution of the average values (Figure 4a) there can be noticed small variations in the geographical space (from 0.85m to 0.88m), with the mention that the southern part of this region seems to be more energetic. Regarding the maximum values (Figure 4b) the south sector reports wave heights of 5.5m more frequently, while for the remaining areas wave conditions of 4.4m can be considered representative.

To identify in more detail the wave conditions which may be representative for the target area, the reference point A1 ($45^{o}10'$N, 30^{o}E) was considered for study. In Figure 5a there are presented the *Hs* histograms corresponding to summer and winter season (from October to March), respectively. From a

first overview it can be noticed that most of the *Hs* values are being reported below 2m (in both seasons), but with a general distribution between the interval 1-1.5m. During the winter time (which is more energetic) the wave conditions from the 1-1.5m interval become dominant, highlighting also the possibility to encounter waves higher than 2m.

In Figure 5b, the monthly evolutions of *Hs* values are presented. Regarding the mean value it can be noticed that the months January and February are more energetic with a maximum average *Hs* value of 1.27m, while *Hs* values of almost 0.5m are being reported during May, June and July. Regarding the maximum wave conditions it can be noticed that these may occur only during the winter season, especially in February (5.5m), January (4m) and November (3.8m). During the summer season a maximum value of 2.3m was reported in June while a minimum of 1.7m is indicated for July.

3. RESULTS AND DISCUSSIONS

Based on the wave conditions identified from the satellite data, two wave propagation patterns were considered. Thus, the first one illustrates the mean wave conditions that may occur in the target area, and they are indicated by a *Hs* value of 0.9m, while the second one correspond to a more energetic wave pattern that may occur especially during the winter time indicated by a *Hs* value of 5.4m. Following the work of Rusu (2009), for the parameters mean period (*Tm*) and mean wave direction (*Dir*), the most relevant patterns were considered for the target area, namely: wave periods of 5s and 8s for the average and energetic wave conditions, respectively. In terms of mean wave direction, the north-eastern sector was indicated as being dominant.

By considering the above wave characteristics, the most significant influences of the hybrid wave-wind farm in the geographical space will be identified for two case studies: CS1 (*Hs*=0.9m, *Tm*=5s, *Dir*=90°) and CS2 (*Hs*=5.4m, *Tm*=8s, *Dir*=30°).

3.1 Evaluation in the geographical and in the spectral space

In order to highlight the impact of the hybrid wave-wind farm in the geographical space for each case study, two different situations were considered: simulation for the case without the hybrid farm (denoted with N0) and simulation for the case when ten groups of hybrid devices (1 wind turbine + 5 NEMOS systems) operate in a single farm (N10).

In order to evaluate the influence of the hybrid wave-wind farm on the local wave field in Figure 2, four reference points were defined. The first control point is a boundary point (denoted with BP) which can provide accurate information regarding the incident wave characteristics without the influence of the hybrid farm. The remaining points (OP1, OP2 and OP3) are also located in the offshore area, being defined in front of the coastline at a distance of 1.8km from the hybrid line configuration. It is expected that these three points to reflect better the variations that may occur in the geographical and in spectral spaces due to the presence of the hybrid farm.

To assess the coastal impact of the wave farm and to evaluate the nearshore currents, seven reference lines (RL) were positioned along the entire coast (RL1 - RL7). The offshore extremities of each reference line are denoted as the nearshore points (NP) and with the help of these points it was possible to perform the analysis of the wave transformation in the nearshore.

In Figures 6 it is illustrated the impact of the hybrid farm on the wave field for the case study CS1 (*Hs*=0.9m, *Tm*=5s, *Dir*=90°). From a first analysis of the wave conditions it can be noticed that in the target area the wave fields of 0.9m are dominant, while close to the shoreline a particular occurrence of 0.3m wave height was found. For the 10N case study (Figure 6b) the wave field behind the hybrid farm decreases to a value 0.7m but near the coastline the wave conditions remain about the same.

For the case study CS2 (*Hs*=5.4m, *Tm*=8s, *Dir*=30°) presented in Figure 7, it can be noticed that in the absence of the hybrid farm (Figure 7a), the wave conditions in the offshore area are dominant by the *Hs* fields of 4.6 m and 4m, while close to the nearshore area two dominant wave fields of 3.7 an 3.2m are reported. Near the coastline area, there is a combined occurrence of the wave fields in the interval 2.8-0.3m. In the presence of the hybrid farm (Figure 7b) it can be noticed that the wave field of 3.7m advances covering the entire area from the vicinity of the wave-wind farm. Also there is a significant increase in the geographical space of the wave field of 3.2m, especially in the lower part of the considered hybrid farm. These results occur mainly because of the sheltering effect which is induced by the hybrid farm which blocks the wave conditions coming from the north-east sector (30^o). Also this wave field is noticed behind each group of hybrid wave-wind systems, gradually increasing till the end of the hybrid wave-wind farm (lower part of the target area). The sheltering effect is provided mostly by the NEMOS WEC systems, but locally it can be noticed that the wind turbine tower can also reduce the wave field with almost 0.2m.

The impact of the hybrid farm in the spectral space (in terms of analyzing the transformation of a JONSWAP spectrum) for the case CS1 is presented in Figure 8. In the boundary point BP is observed the JONSWAP spectrum in its standard form (with a single peak) and with a maximum energy value of $0.44m^2$/Hz/deg, while for the point OP2 similar values are observed. In the presence of the hybrid farm, the single peak JONSWAP spectrum is transformed in a double peak spectrum for the point OP2 while the energy decrease with almost $0.08m^2$/Hz/deg. For the reference point NP3 no significant changes of the spectral shape are observed for the considered configurations (N0 and N10).

For the study case CS2 (Figure 9) the differences on the spectral space become more evident due to the presence of the hybrid farm and of incident wave angle (30°) which interact more with the lateral side of the farm. As a result for the point OP2 the maximum energy spectrum decrease from $17m^2$/Hz/deg to $14m^2$/Hz/deg (N10), while in the directional space small differences are observed.

In Table 1 a detailed data representation in relationship with the variation of the wave parameters is given for the two case studies, CS1 and CS2, respectively. In the above table, the values for the all references points defined (BP, OP1, OP2, OP3,) corresponding to the two configurations considered (N0 and N10) are presented. The parameters considered in this table are: significant wave height (*Hs*), maximum variance (*Emax*), mean wave direction (*Dir*), directional spreading (DSPR), peak period (*Tp*), mean period (*Tm*), wave length (*Wlen*), the components of the energy transport (*Px, Py*) and the components of the wave forces (*Fx, Fy*).

As we can see in Table 1 the difference of the wave heights *Hs* between the two situations (with and without the hybrid farm) is not so important, but we can notice that the influence is higher when the direction of the wave is of 90°. Also in all the offshore points it is a low decrease of the maximum variance and a higher change of the mean wave direction is present when the wave direction is from 30°.

The results presented in Table 2 show that the significant wave height (*Hs)* is almost the same, the differences being very low. A reason may be because the hybrid farm is deployed at a relatively big distance to the coastline. In relationship with the maximum variance, also there were not registered many differences, the decreasing in the presence of the farm being insignificant.

Table 3 present comprehensive evaluations of the wave parameters for the wave characteristics *Hs*=5.4m, *Tm*=8s, for the case when the incident wave occur from the north-east (30^o) and east (90^o) sector. For the *Hs* value it can be noticed that a maximum value of 4.8m (N0 and N10) is reported for the point BP when the waves arrive from the north-east sector while in the presence of the hybrid farm all the offshore points report values close to 3.7m for both wave directions. Regarding the *Emax* value it can be noticed that in the case of N10, when waves arrive from the north-east sector, this value decreases from 21.32m^2/Hz/deg (reported in BP) to a 13.24m^2/Hz/deg indicated for the point OP3. When the waves arrive from the east sector, the point OP2 reported the lowest value (15.36m^2/Hz/deg).

By analyzing the wave direction, the points OP1 and OP2 report a difference of 4.8^o between the cases N0 and N10 when the waves arrive from the north-west sector, while a maximum difference of 2^o is observed for the point OP3 when the waves arrive from east. In relationship with DSPR, wave length and period, small differences are reported between the BP control point and the nearshore points. For the wave energy component, a maximum value of 6.26m^3/s is reported by the point BP for the *Py* component (north-west wave) while a value of about 6.7m^3/s is reported by the points OP2 and OP3 when the waves arrive from east. A maximum value of 0.48 N/m^2 is reported in the point OP1 (N0 and N10), for the incident waves coming from the north-east sector.

From the analysis of nearshore points presented in the Table 4 it can be noticed that there are very small variations between the cases N0 and N10, even in the case when the wave conditions from CS2 are more energetic. By considering also the results presented in Table 2 it can be noticed that the dissipative effect, which is specific to the shallow water area, becomes dominant near the coastline, while the influence of a hybrid farm located in the offshore area represents an insignificant factor.

Since another purpose of the present work is to evaluate the impact of the incident wave field on a direct contact with the wave-wind farm, this evaluation is carried out by considering three reference lines crossing the hybrid farm as it can be seen in Figure 10.

The evolution of the waves for the two situations N0 (blue) and N10 (red) are presented in figures 12 (for Line 1), 13 (for Line 2) and 14 (for Line 3) together with the corresponding bathymetric profiles corresponding to each line. From all the above figures it can be noticed the presence of the hybrid farm which reduces the incident wave field, and also the fact that close to the coastline area those difference are greatly reduced. For the case SC1, line L3 reports a maximum difference of 0.4m

(from 0.9m to 0.5m), while a minimum value of 0.15m (from 0.9m to 0.75m) is registered by the line L2. For the study case CS2 there is a maximum difference of 1m (from 4.1m to 3.1m), while a minimum value of 0.3m (from 4.1m to 3.8m) is also reported for the line L2.

3.2 Assessment of the impact on the shoreline dynamics

In ISSM modeling system, the nearshore currents were evaluated along the reference lines RL1-RL7, for the two different configurations (N0 and N10). Regarding the maximum current velocity, Table 5 illustrates the results corresponding to wave condition *Hs*=0.9m, *Tm*=5s and two different wave directions (30° and 90°) while Table 6 presents the current velocity values based on the combination: *Hs*=5.4m, *Tm*=8s (for the same wave directions).

From Table 5 it can be noticed that the maximum value is reported for the line L1 with 1.09m/s from the 30^o direction (N0 and N10), while a minimum value of 0.02m/s is observed at the line L4 in the case of waves coming from a 90^o direction. Similar, in the Table 6 the line L1 is indicated as being more energetic with a value of 1.56m/s, while this time the lowest value is being reported at the line L6 with a value of 0.04m/s (for N0 and N10). A graphical evolution of the current speeds for the considered study cases is presented in Figure 14.

4. FINAL CONSIDERATION

In the near future the renewable energy portfolio is expected to extend rapidly in the offshore areas. From this perspective, the evaluation of the coastal influence of such energy projects that can operate in the nearshore represents a very actual problem. Regarding this aspect, the present work shows an evaluation of the changes expected to be induced in the coastal wave climate by a hybrid wave-wind energy farm. The target area has been chosen on the western side of the Black Sea where more energetic wave conditions were reported

Evaluations were carried out in both geographical and spectral spaces for some relevant wave patterns corresponding to two different situations: without and with the presence of the hybrid farm, respectively. The results show that near the farm there have been observed changes that occur in the wave fields but these differences gradually attenuate towards the coast.

In order to assess better the changes taking place in the spectral shapes due to the energy farm, for each case study considered transformations of theoretical JONSWAP spectra were followed. In this analysis, changes of the wave spectra have been observed and at the wave direction of 90° the single peaked wave spectra were changed by the hybrid farm in double peaked spectra in the vicinity of the hybrid farm.

By using the modeling system ISSM that joins SWAN with the 1D surf model, the changes induced in the shoreline dynamics were investigated in order to identify the wave farm impact in terms of longshore currents. The results show that the nearshore waves are not very much affected by the presence of the hybrid farm, being more affected by the dissipation processes which commonly occur in the shallow water areas. Regarding the current velocities, although the wave-wind farm induce

significant variations (especially for the CS2), from the analyses performed it seemed that the current speeds depend more on the local bathymetry configuration corresponding to each reference point.

On the other hand, although the presence of the hybrid farm leads in general to a gradually decrease of the wave conditions its influence at the level of the shoreline dynamics may lead to also to some enhancements of the longshore current velocity. This means that due to the particularities of the target area and due to the spatial configuration of the hybrid farm (parallel with the coastline) some coastal processes can be also accentuated instead of being attenuated.

ACKNOWLEDGMENT

The work of the first two authors has been made in the scope of the project SOP HRD - EFICIENT 61445/2009 (Management System for the Fellowships Granted to the PhD Students).

REFERENCES

1. Booij N, Ris R C, Holthuijsen L H (1999). A third generation wave model for coastal regions. Part 1: Model description and validation, J. Geophys.Res 104(4):7649-7666.

2. Conley D C, Rusu E (2006a). The middle way of surf modeling 2006a, Proceedings of the 30th International Conference on Coastal Engineering ICCE 2006, 2-9 September, San Diego, USA.Published in World Scientific Pub Co Inc, Coastal Engineering: 1053-1065.

3. Conley D C, Rusu E (2006b). Tests of wave shoaling and surf models in a partially enclosed basin. Maritime Transportation and Exploitation of Ocean and Coastal Resources: 1015-1021.

4. Dan S, Stive M J F, van der Westhuysen A (2007). Alongshore Sediment Transport Capacity Computation on the Coastal Zone of the Danube Delta using the Simulated Wave Climate. GeoEcoMarina, 13: 21-30.

5. Dibarboure G, Dorandeu J, Le Traon PY, et al (2006). SSALTO/DUACS: 15 years of precise and consistent multi-mission altimetry data. European Space Agency, (Special Publication) ESA SP 614.

6. ELSAM (2002). Horns Rev offshore wind farm. Ground-breaking wind power plant in the North Sea.

7. EWEA (European Wind Energy Association) (2012). The European offshore wind industry key 2011 trends and statistics.

8. Gaspar P, Labroue S, Ogor F, et al (2002). Improving nonparametric estimates of the sea state bias in radar altimetry measurements of sea level. J Atmos Ocean Tech 19: 1690-1707.

9. Gâştescu P, Driga B (2012). Morphological changes of the Romanian Black Sea accumulation coast. International conference Water resources and wetlands, 14-16 September 2012, Tulcea - Romania: 379-389.

10. Li M, Raymond I, Wolf J, et al (2011). Numerical investigation of wave propagation in the Liverpool Bay, NW England. Acta Oceanologica Sinica, 30(5):1-13.

11. Liang B, Zhao H, Li H, et al (2012). Numerical study of three-dimensional wave-induced longshore current's effects on sediment spreading of the Huanghe River mouth. Acta Oceanologica Sinica, 31(2): 129-138.

12. Longuet-Higgins M S (1970). Longshore currents generated by obliquely incident sea waves, I and II. J. Geophys. Res, 75: 6778-6801.

13. Marchand M (2010). Concepts and Science for Coastal Erosion Management. Concise report for policy makers. Deltares, Delft.

14. Mettlach T R, Earle M D, Hsu Y L (2002). Software design document for the Navy Standard Surf Model, Version 3.2. Naval Research Laboratory, Stennis Space Center, Mississippi.

15. NEMOS (2012). http://www.nemos.org/home/ (accessed January 2013).

16. Onea F, Rusu E (2012). Wind energy assessments along the Black Sea basin. Meteorological Applications, DOI: 10.1002/met.1337.

17. Policy Research Corporation (PRC) (2009). The economics of climate change adaptation in EU coastal areas - Romania.

18. Rusu E, Guedes Soares, C (2010). Validation of two wave and nearshore current models. Journal of Waterway, Port, Coastal, and Ocean Engineering, 136(1): 27-45.

19. Rusu E, Măcuță S (2009). Numerical modelling of longshore currents in marine environment. Environmental Engineering and Management Journal, 8(1): 147-151.

20. Rusu E (2009). Wave energy assessments in the Black Sea. J Mar Sci Tech 14: 359-372.

21. Rusu E (2010a). Modelling of wave-current interactions at the Danube's mouths, Journal of Marine Science and Technology, 15(2):143-159.

22. Rusu L (2010b). Application of numerical models to evaluate oil spills propagation in the coastal environment of the Black Sea, Journal of Environmental Engineering and Landscape Management; 18: 288-295.

23. Rusu L, Ivan A (2010). Modelling Wind Waves in the Romanian Coastal Environment. Environmental Engineering and Management Journal, 9(4), 547-552.

24. Snyder B, Kaiser M J (2009). Ecological and economic cost - benefit analysis of offshore wind energy. Renewable Energy 34 (6): 1567-1578.

25. Stockdon H F, Doran K J, Thompson D M, et al (2012). National assessment of hurricane-induced coastal erosion hazards: Gulf of Mexico: U.S. Geological Survey Open-File Report 2012-1084.

26. Strauss D, Mirferendesk H, Tomlinson R (2007). Comparison of two wave models for Gold Coast, Australia. Journal of Coastal Research, Special Issue 50: 312-316.

27. Svendsen I A, Haas K, Zhao Q (2002). Quasi-3D Nearshore circulation model SHORECIRC, version 2.0. Center for Applied Coastal Research, University of Delaware.

28. Yang J, Zhang J, Meng J (2010). A detection model of underwater topography with a series of SAR images acquired at different time. Acta Oceanologica Sinica, 29 (4): 28-37.

29. Yin X, Qiao F, Xia C, et al (2010). Reconstruction of eddies by assimilating satellite altimeter data into Princeton Ocean Model. Acta Oceanologica Sinica, 29(1):1-11.

LIST OF FIGURES

points and RL represent the reference lines considered for the analysis of the nearshore currents. Each offshore extremity point of the above reference lines is denoted as NP (nearshore point).

Figure 3: Spatial configuration of the considered hybrid wave-wind farm, where: a) 10 wind turbines and 50 NEMOS systems, b) 1 wind turbine and 5 NEMOS systems, and c) NEMOS WEC system (source http://www.nemos.org/home/).

Figure 4: Spatial distributions of the significant wave height (*Hs*) conditions in the western part of the Black Sea based on the satellite data for the time interval December 2005-July 2012. The maps correspond to: a) mean values (m) and b) maximum values (m).

Figure 5: Analysis of the *Hs* values based on the satellite data for the reference point A1, for the time interval December 2005-July 2012, where: a) *Hs* histograms for the summer and winter time and b) monthly evolution of the average and maximum *Hs* values.

Figure 6: Evaluation in the geographical space of the impact on the wave field of a hybrid farm that operates in the target area. CS1 – average to high energetic conditions and waves coming from east (90° in nautical convention), where: a) SWAN simulation for the case without hybrid farm (N0). b) SWAN simulation for the case when a hybrid wave-wind farms operate in line (N10). The *Hs* scalar fields are presented in background while in foreground the wave vectors are indicated.

Figure 7: Evaluation in the geographical space of the impact on the wave field of a hybrid farm that operates in the target area. CS2 – high energetic conditions and waves coming from northeast (30° in nautical convention), where: a) SWAN simulation for the case N0. b) SWAN simulation for the case N10. The *Hs* scalar fields are presented in background while in foreground the wave vectors are indicated.

Figure 8: Evaluation in the spectral space of the impact on the wave field of a hybrid farm that operates in the target area for CS1, where: a) BP for N0. b) OP2 for N0. c) NP3 for N0, d) OP2 for N10, e) NP3 for N10.

Figure 9: Evaluation in the spectral space of the impact on the wave field of a hybrid farm that operates in the target area for CS2, where: a) BP for N0. b) OP2 for N0. c) NP3 for N0, d) OP2 for N10, e) NP3 for N10.

Figure 10: Evaluation of the impact of the energy farms on the maximum velocities of the nearshore currents along the reference lines considered, where: a) CS1 and b) CS2.

Figure 11: *Hs* variation along the reference line 1 without and with hybrid farm (N0, N10) for the two cases considered (CS1 and CS2) and the variation of the water depth along the reference line.

Figure 12: *Hs* variation along the reference line 2 without and with hybrid farm (N0, N10) for the two cases considered (CS1 and CS2) and the variation of the water depth along the reference line.

Figure 13: *Hs* variation along the reference line 3 without and with hybrid farm (N0, N10) for the two cases considered (CS1 and CS2) and the variation of the water depth along the reference line.

Figure 14: Evaluation of the impact of the energy farms on the maximum velocities of the nearshore currents along the reference lines considered: where: a) CS1 and b) CS2.

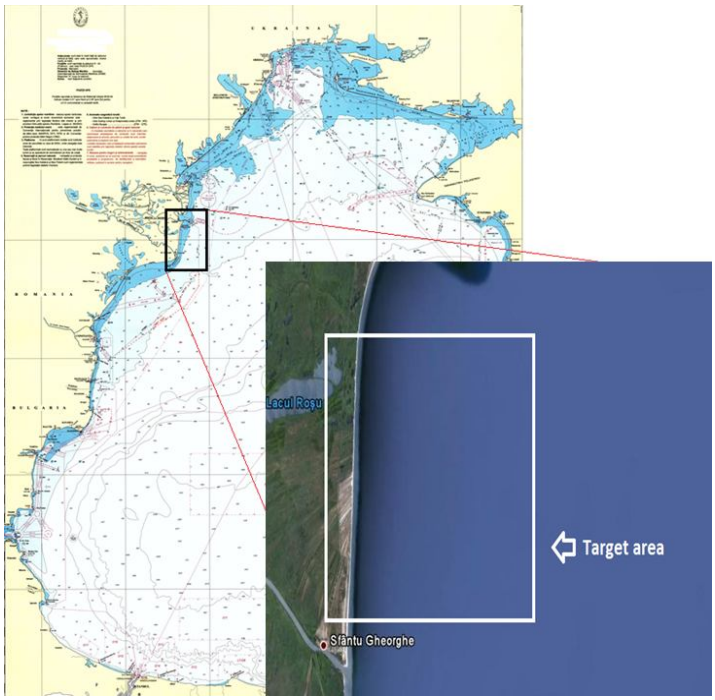

Figure 1

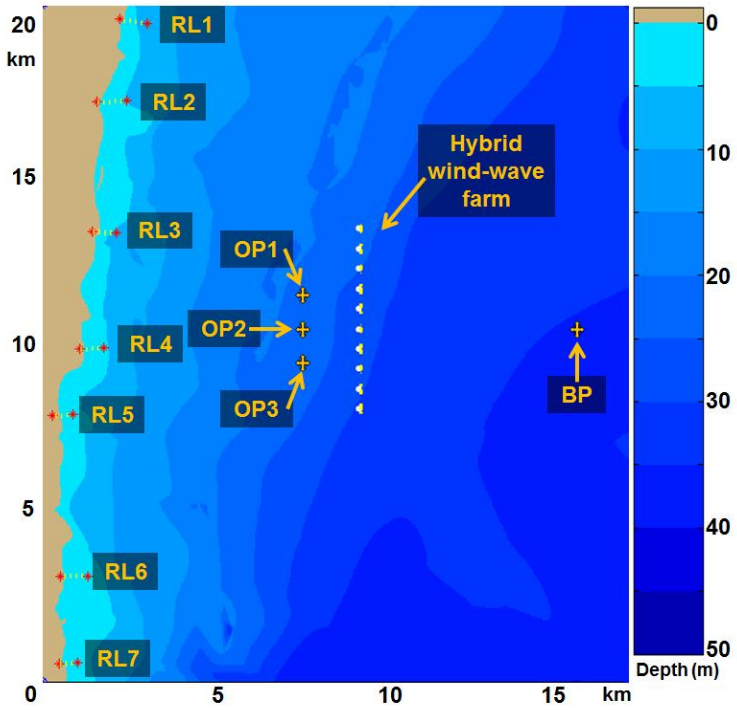

Figure 2

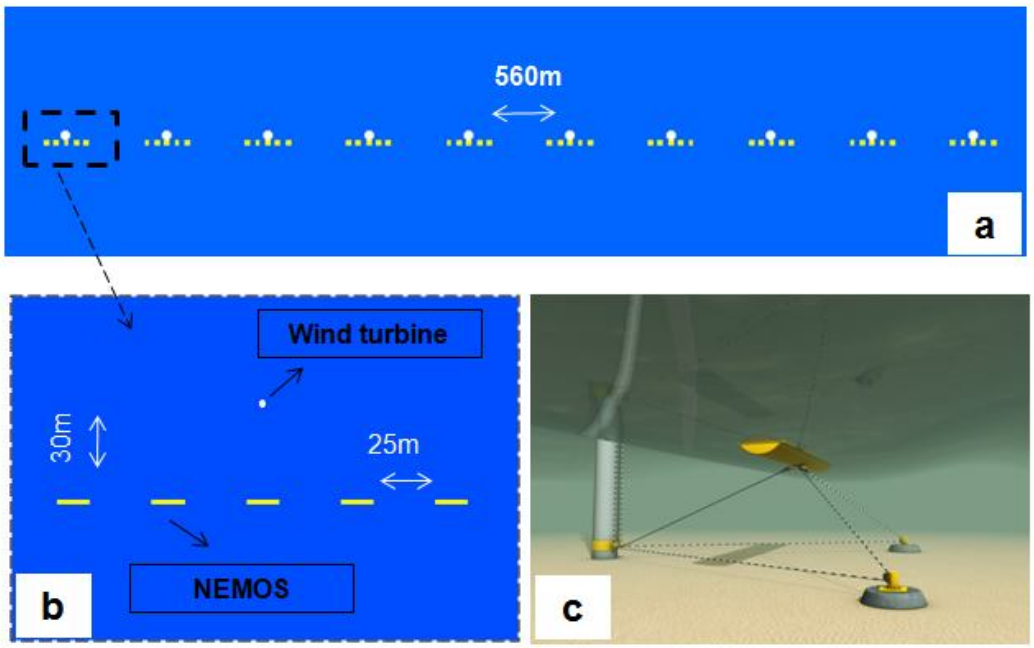

Figure 3

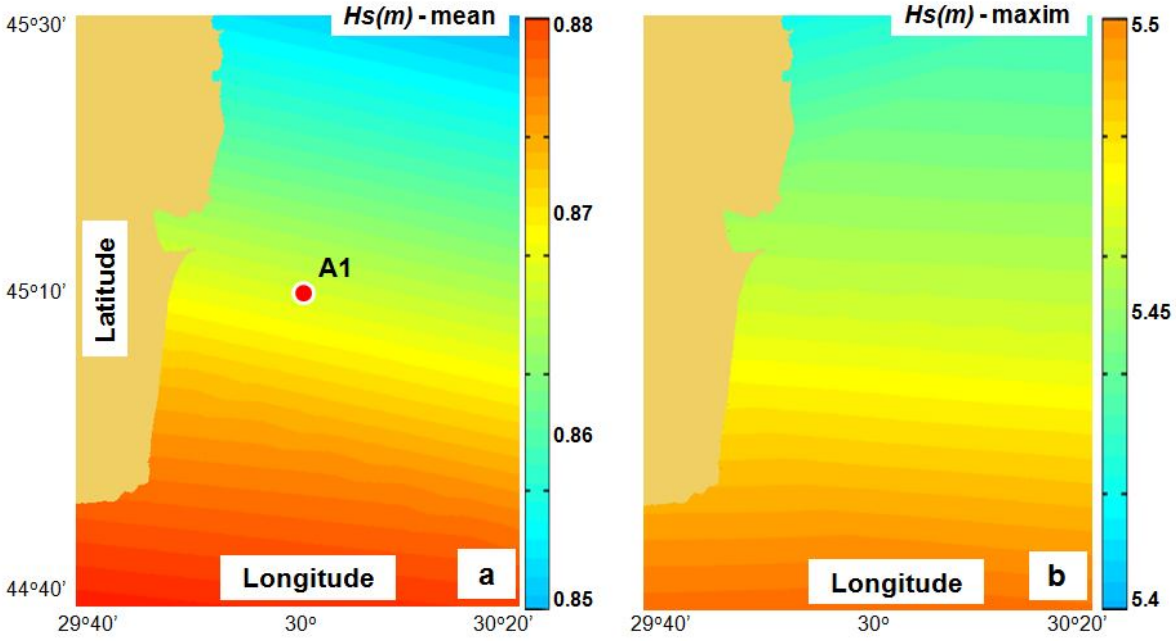
Hs(m) - mean
Hs(m) - maxim
45°30'
45°10'
44°40'
Latitude
A1
Longitude
a
b
0.88
0.87
0.86
0.85
5.5
5.45
5.4
29°40'
30°
30°20'

Figure 4

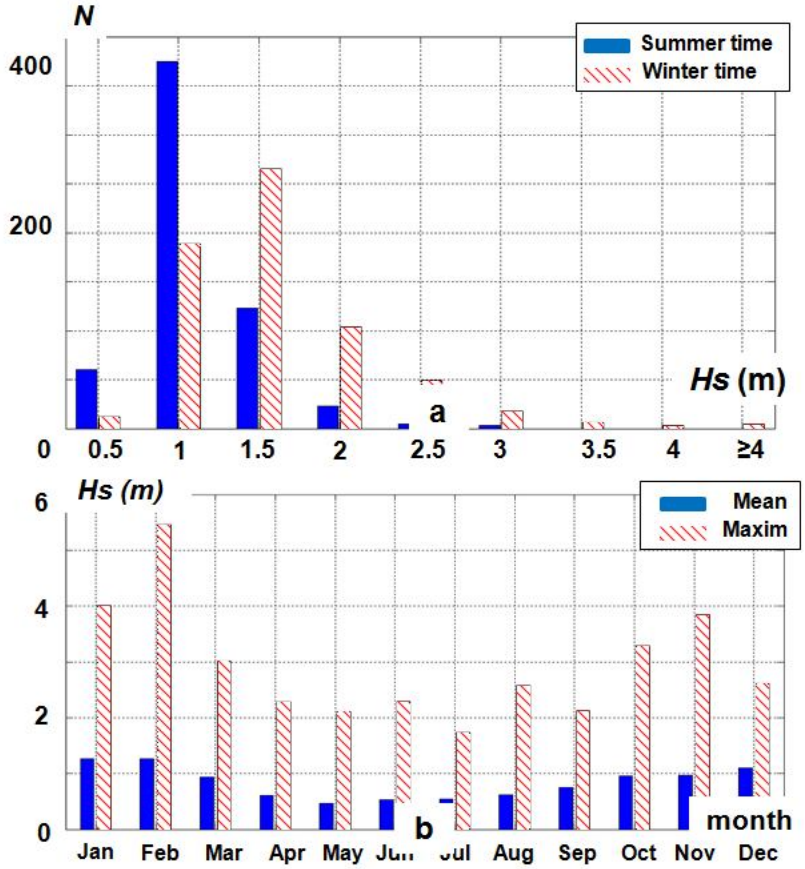
N
Summer time
Winter time
Hs (m)
a
0.5
1
1.5
2
2.5
3
3.5
4
≥4
Hs (m)
Mean
Maxim
month
b
Jan
Feb
Mar
Apr
May
Aug
Sep
Oct
Nov
Dec

Figure 5

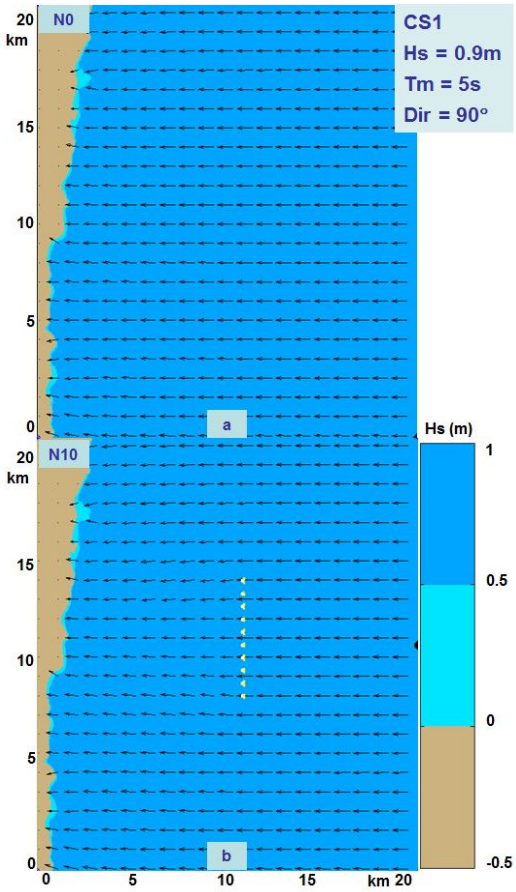

Figure 6

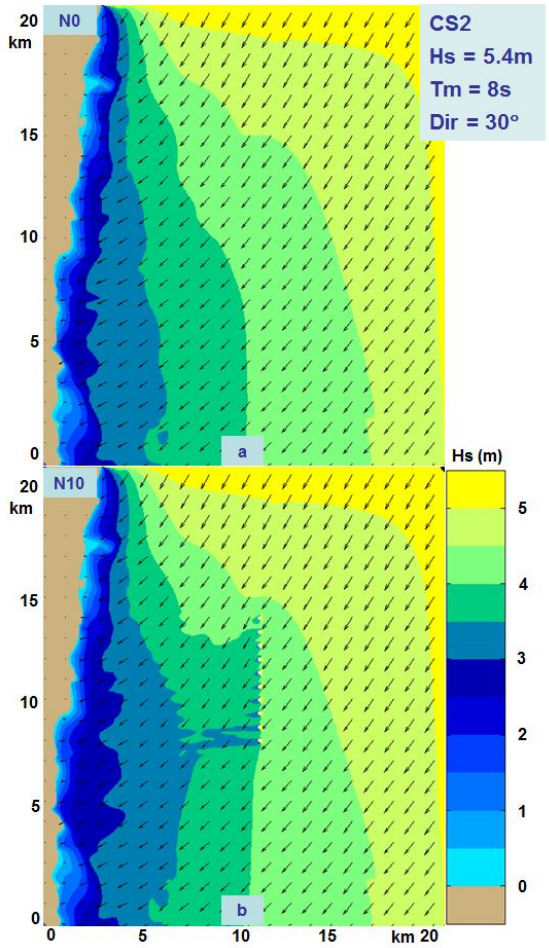
N0
CS2
Hs = 5.4m
Tm = 8s
Dir = 30°
a
N10
b
Hs (m)
20
km
15
10
5
0
0
5
10
15
km 20
4
3
2
1

Figure 7

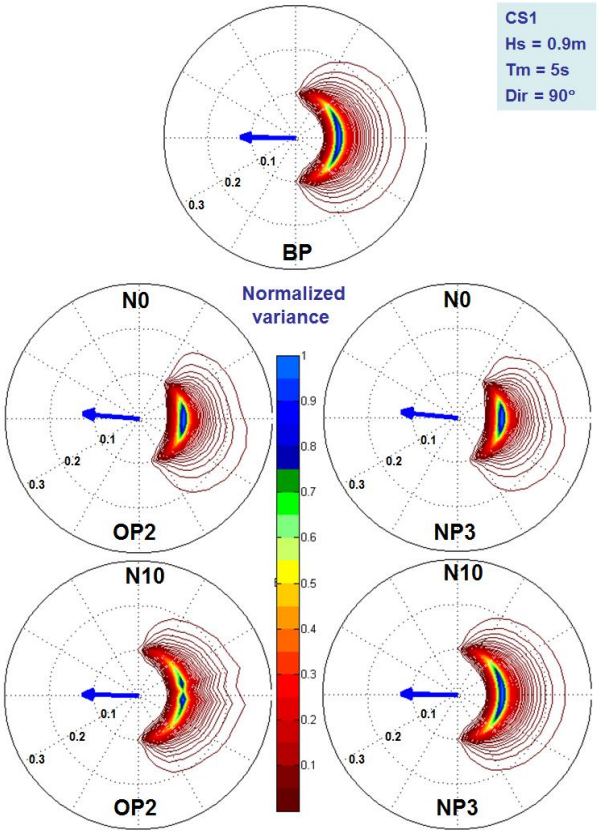
CS1
Hs = 0.9m
Tm = 5s
Dir = 90°
BP
N0
OP2
N0
NP3
N10
OP2
N10
NP3
Normalized variance
1
0.9
0.8
0.7
0.6
0.5
0.4
0.3
0.2
0.1
0.1
0.2
0.3

Figure 8

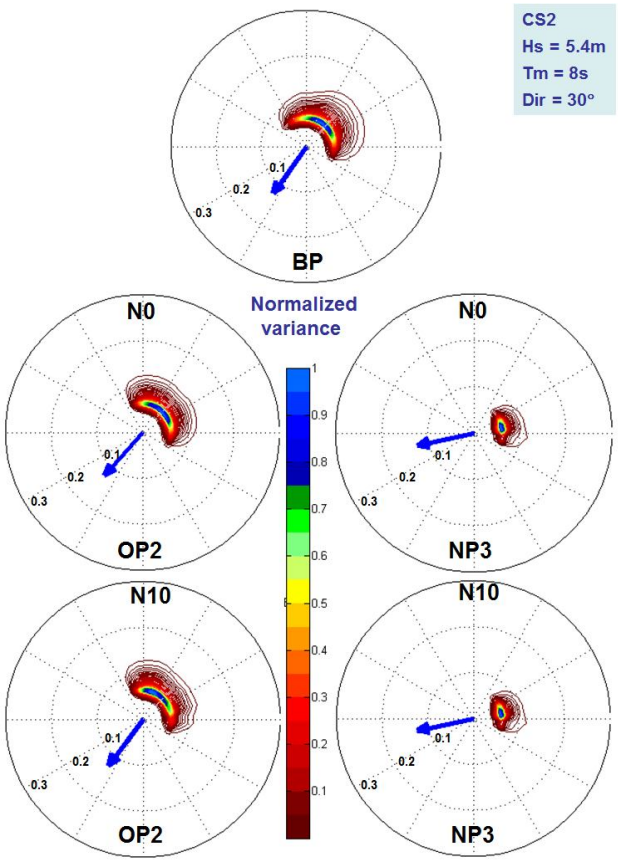
CS2
Hs = 5.4m
Tm = 8s
Dir = 30°
BP
N0
OP2
N0
NP3
N10
OP2
N10
NP3
Normalized variance
1
0.9
0.8
0.7
0.6
0.5
0.4
0.3
0.2
0.1
0.1
0.2
0.3

Figure 9

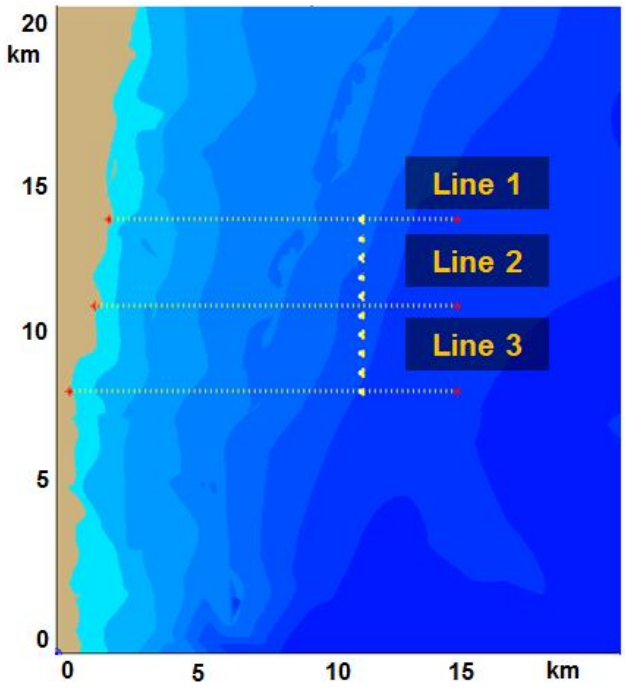

Figure 10

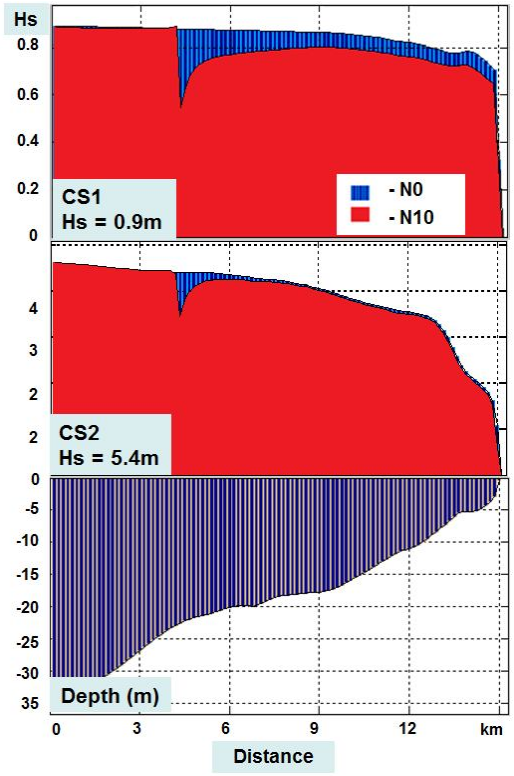

Figure 11

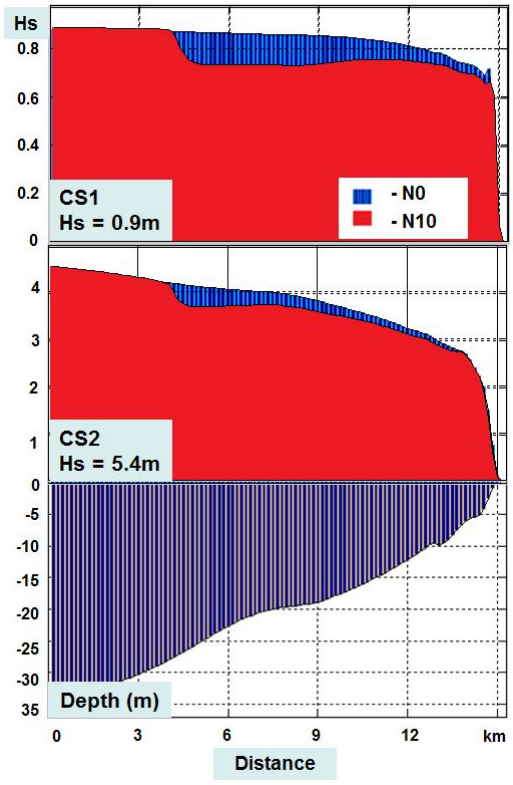
Hs
0.8
0.6
0.4
0.2
0
CS1
Hs = 0.9m
- N0
- N10
4
3
2
1
0
-5
-10
-15
-20
-25
-30
35
CS2
Hs = 5.4m
Depth (m)
0
3
6
9
12
km
Distance

Figure 12

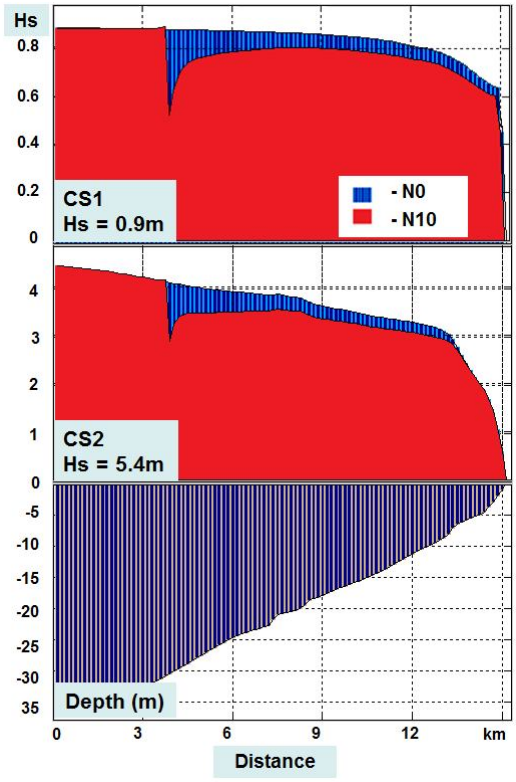
Hs
0.8
0.6
0.4
0.2
0
CS1
Hs = 0.9m
- N0
- N10
4
3
2
1
0
-5
-10
-15
-20
-25
-30
35
CS2
Hs = 5.4m
Depth (m)
0
3
6
9
12
km
Distance

Figure 13

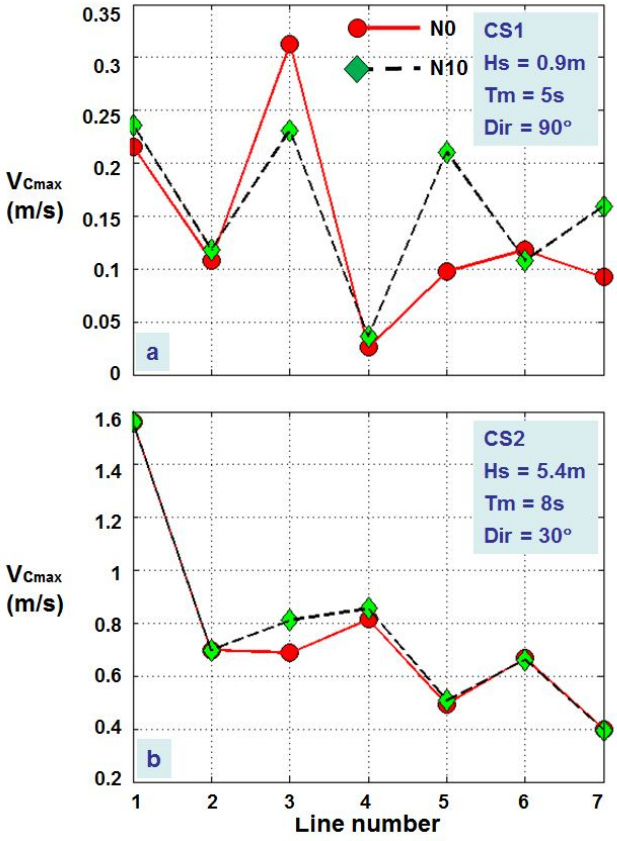

Figure 14

LIST OF TABLES

Table 1

N	Hs (m)	Emax (m^2/Hz/deg)	Dir (deg)	DSPR (deg)	Tm/Tp (s)	Wlen (m)	Px (m^3/s)	Py (m^3/s)	Fx (N/m^2)	Fy (N/m^2)

a) Direction: 30°											
BP	N0	0.9	0.44	90.0	33.19	4.2/4.9	24.4	-0.15	0	0	0
	N10	0.9	0.44	90.0	34.82	4.2/4.9	24.4	-0.15	0	0	0
OP1	N0	0.8	0.43	33.4	30.88	4.3/4.9	26.3	-0.08	-0.11	0	0
	N10	0.8	0.42	28.5	30.27	4.3/4.9	26.2	-0.06	-0.10	0	0
OP2	N0	0.8	0.43	34.1	30.50	4.3/4.9	26.4	-0.08	-0.11	0	0
	N10	0.8	0.40	29.0	30.35	4.3/4.9	26.2	-0.06	-0.10	0	0
OP3	N0	0.8	0.42	34.9	30.10	4.3/4.9	26.5	-0.08	-0.11	0	0
	N10	0.7	0.40	30.0	30.25	4.3/4.9	26.3	-0.05	-0.09	0	0
b) Direction: 90°											
OP1	N0	0.9	0.43	90.1	33.06	4.3/4.9	26.6	-0.14	0	0	0
	N10	0.7	0.37	89.3	34.50	4.3/4.9	26.5	-0.10	0	0	0
OP2	N0	0.9	0.43	90.2	33.06	4.3/4.9	26.7	-0.14	0	0	0
	N10	0.7	0.35	90.8	34.55	4.3/4.9	26.5	-0.10	0	0	0
OP3	N0	0.9	0.43	90.3	33.08	4.3/4.9	26.7	-0.14	0	0	0
	N10	0.7	0.42	92.3	34.83	4.3/4.9	26.5	-0.10	0	0	0

Table 2

	N	Hs (m)	Emax (m^2/Hz/deg)	Dir (deg)	DSPR (deg)	Tm/Tp (s)	Wlen (m)	Px (m^3/s)	Py (m^3/s)	Fx (N/m^2)	Fy (N/m^2)
NP1	N0	0.8	0.42	83.6	28.50	4.2/4.9	21.8	-0.14	-0.02	0.17	0.04
	N10	0.8	0.42	82.5	27.99	4.2/4.9	21.7	-0.14	-0.02	0.17	0.04
NP2	N0	0.7	0.45	90.8	22.82	4.2/4.9	21.4	-0.11	0	0.20	0.05
	N10	0.7	0.44	88.7	22.91	4.2/4.9	21.1	-0.10	0	0.18	0.05
NP3	N0	0.7	0.43	94.6	23.90	4.2/4.9	19.1	-0.11	0.01	0.07	0.26
	N10	0.7	0.43	95.2	23.58	4.2/4.9	19.0	-0.11	0.01	0.07	0.26
NP4	N0	0.7	0.49	90.4	22.60	4.2/4.9	20.1	-0.11	0	0.26	0.05
	N10	0.7	0.36	90.7	24.22	4.2/4.9	19.9	-0.10	0	0.22	0.05
NP5	N0	0.7	0.40	93.9	22.72	4.2/4.9	21.0	-0.11	0.01	0.17	0
	N10	0.6	0.38	96.1	23.19	4.2/4.9	20.8	-0.09	0.01	0.15	0
NP6	N0	0.7	0.41	81.8	22.40	4.2/4.9	20.7	-0.11	-0.02	-0.03	0.01
	N10	0.7	0.41	83.1	22.22	4.2/4.9	20.6	-0.10	-0.01	-0.03	0.01
NP7	N0	0.7	0.43	94.6	23.90	4.2/4.9	19.1	-0.11	0.01	0.07	0.26
	N10	0.7	0.43	95.2	23.58	4.2/4.9	19.1	-0.11	0.01	0.07	0.26

Table 3

	N	Hs (m)	Emax (m^2/Hz/deg)	Dir (deg)	DSPR (deg)	Tm/Tp (s)	Wlen (m)	Px (m^3/s)	Py (m^3/s)	Fx (N/m^2)	Fy (N/m^2)
a) Direction: 30°											
BP	N0	4.8	21.32	35.3	32.06	7.2/8.3	74.4	-4.36	-6.26	-0.12	-0.22
	N10	4.8	21.32	35.0	32.72	7.2/8.3	74.4	-4.32	-6.27	-0.12	-0.22
OP1	N0	4.1	17.11	40.3	29.26	7.3/8.3	74.8	-4.18	-4.83	0.48	-0.28
	N10	3.8	15.43	35.5	29.03	7.3/8.3	74.3	-3.18	-4.35	0.48	-0.22
OP2	N0	4.1	17.02	41.5	28.73	7.3/8.3	74.7	-4.10	-4.55	0.40	-0.20
	N10	3.7	14.05	36.7	28.99	7.3/8.3	74.1	-2.99	-3.92	0.39	-0.22
OP3	N0	4.0	16.88	43.0	28.53	7.3/8.3	75.0	-4.11	-4.32	0.34	-0.31
	N10	3.6	13.24	38.5	29.09	7.3/8.3	74.3	-2.96	-3.62	0.33	-0.24
b) Direction: 90°											
OP1	N0	4.2	19.20	92.8	30.18	7.3/8.3	74.7	-6.50	0.36	0.44	-0.07
	N10	3.6	16.50	92.3	31.63	7.3/8.3	74.0	-4.61	0.22	0.36	0.05
OP2	N0	4.2	18.95	93.2	30.10	7.3/8.3	75.2	-6.64	0.41	0.39	-0.03
	N10	3.6	15.36	94.0	31.58	7.3/8.3	74.5	-4.67	0.35	0.35	-0.04
OP3	N0	4.3	18.64	93.8	30.26	7.3/8.3	75.7	-6.70	0.48	0.35	-0.21
	N10	3.7	17.48	95.8	32.01	7.3/8.3	75.2	-4.77	0.51	0.37	-0.10

Table 4

	N	Hs (m)	Emax (m^2/Hz/deg)	Dir (deg)	DSPR (deg)	Tm/Tp (s)	Wlen (m)	Px (m^3/s)	Py (m^3/s)	Fx (N/m^2)	Fy (N/m^2)
NP1	N0	2.4	6.88	48.9	26.31	7.3/8.3	47.2	-1.43	-1.24	-3.51	-3.09
	N10	2.4	6.88	48.9	26.31	7.3/8.3	47.2	-1.43	-1.24	-3.51	-3.09
NP2	N0	2.2	15.41	72.6	12.11	7.5/8.3	46.9	-1.57	-0.49	-5.42	-1.41
	N10	2.2	15.52	72.4	11.88	7.5/8.3	47.0	-1.56	-0.50	-5.39	-1.41
NP3	N0	1.6	7.78	77.8	12.46	7.5/8.3	41.1	-0.75	-0.16	-2.69	-0.16
	N10	1.6	7.88	78.0	12.43	7.5/8.3	41.0	-0.75	-0.16	-2.68	-0.15
NP4	N0	1.7	8.58	77.7	13.52	7.5/8.3	40.8	-0.91	-0.20	-6.30	-1.40
	N10	1.7	8.94	75.6	13.46	7.5/8.3	41.0	-0.89	-0.23	-6.16	-1.48
NP5	N0	1.8	9.91	76.8	12.85	7.5/8.3	44.7	-1.05	-0.25	-1.63	-0.73
	N10	1.8	9.14	76.1	13.36	7.5/8.3	44.4	-1.03	-0.26	-1.43	-0.66
NP6	N0	1.8	10.00	67.0	14.32	7.4/8.3	44.4	-1.03	-0.44	-2.63	-1.25
	N10	1.8	9.41	67.2	14.62	7.4/8.3	44.3	-1.03	-0.43	-2.59	-1.22
NP7	N0	1.6	7.78	77.8	12.46	7.5/8.3	41.1	-0.75	-0.16	-2.69	-0.16
	N10	1.6	7.88	78.0	12.43	7.5/8.3	41.0	-0.75	-0.16	-2.68	-0.15

Table 5

Case study	Line config.	L1	L2	L3	L4	L5	L6	L7
H0.9D30	N0	1.09	0.36	0.67	0.31	0.46	0.29	0.43
	N10	1.09	0.36	0.68	0.30	0.45	0.27	0.41
H0.9D90	N0	0.22	0.11	0.31	0.02	0.10	0.12	0.09
	N10	0.24	0.12	0.23	0.04	0.21	0.11	0.16

Table 6

Case study	Line config.	L1	L2	L3	L4	L5	L6	L7
H5.4D30	N0	1.56	0.70	0.69	0.82	0.49	0.67	0.40
	N10	1.56	0.70	0.81	0.86	0.51	0.66	0.40
H5.4D90	N0	0.19	0.07	1.35	0.52	0.40	0.04	0.50
	N10	0.34	0.10	1.31	0.53	0.41	0.04	0.50